



**HAL**  
open science

## **SrCu(OH)<sub>3</sub>Cl, an isolated equilateral triangle spin S=1/2 model system**

Sudip Pal, Petr Doležal, Scott A Strøm, Sylvain Bertaina, Andrej Pustogow,  
Reinhard K Kremer, Martin Dressel, Pascal Puphal

► **To cite this version:**

Sudip Pal, Petr Doležal, Scott A Strøm, Sylvain Bertaina, Andrej Pustogow, et al.. SrCu(OH)<sub>3</sub>Cl, an isolated equilateral triangle spin S=1/2 model system. *Physical Review Research*, 2024, 6 (3), pp.0303027. 10.1103/PhysRevResearch.6.033027. hal-04639528

**HAL Id: hal-04639528**









**<https://hal.science/hal-04639528v1>**

Submitted on 9 Jul 2024

**HAL** is a multi-disciplinary open access archive for the deposit and dissemination of scientific research documents, whether they are published or not. The documents may come from teaching and research institutions in France or abroad, or from public or private research centers.

L'archive ouverte pluridisciplinaire **HAL**, est destinée au dépôt et à la diffusion de documents scientifiques de niveau recherche, publiés ou non, émanant des établissements d'enseignement et de recherche français ou étrangers, des laboratoires publics ou privés.

**SrCu(OH)<sub>3</sub>Cl, an isolated equilateral triangle spin  $S = 1/2$  model system**

Sudip Pal <sup>1,\*</sup> Petr Doležal <sup>2,3</sup> Scott A. Strøm <sup>3</sup> Sylvain Bertaina <sup>4</sup> Andrej Pustogow <sup>3</sup> Reinhard K. Kremer <sup>5,†</sup>  
Martin Dressel <sup>1,‡</sup> and Pascal Puphal <sup>5,§</sup>

<sup>1</sup>*Physikalisches Institut, Universität Stuttgart, Pfaffenwaldring 57, 70569 Stuttgart, Germany*

<sup>2</sup>*Department of Condensed Matter Physics, Faculty of Mathematics and Physics, Charles University, Ke Karlovu 5, 121 16 Prague 2, Czech Republic*

<sup>3</sup>*Institute of Solid State Physics, TU Wien, 1040 Vienna, Austria*

<sup>4</sup>*CNRS, Aix-Marseille Université, IM2NP (UMR 7334), Institut Matériaux Microélectronique et Nanosciences de Provence, Marseille, France*

<sup>5</sup>*Max-Planck-Institute for Solid State Research, Heisenbergstraße 1, 70569 Stuttgart, Germany*



(Received 22 January 2024; accepted 14 June 2024; published 8 July 2024)

We have investigated the magnetic ground state properties of the quantum spin trimer compound strontium hydroxy copper chloride SrCu(OH)<sub>3</sub>Cl using bulk magnetization, specific heat measurements, nuclear magnetic resonance (NMR), and electron spin resonance (ESR) spectroscopy. SrCu(OH)<sub>3</sub>Cl consists of layers with isolated Cu<sup>2+</sup> triangles and hence provides an opportunity to understand the magnetic ground state of an isolated system of  $S = 1/2$  arranged on an equilateral triangle. Although magnetization measurements do not exhibit a phase transition to a long-range ordered state down to  $T = 2$  K, they reveal the characteristic behavior of isolated trimers with an exchange of  $J = 154$  K. The Curie-Weiss behavior changes around 50–80 K, as is also seen in the NMR spin-lattice relaxation rate. In zero magnetic field, our specific heat data establish a second-order phase transition to an antiferromagnetic ground state below  $T = 1.2$  K. We have drawn a magnetic field-temperature ( $H$ - $T$ ) phase diagram based on the specific heat measurements. The ESR data show divergence of the linewidth at lower temperatures, which precedes the phase transition to an antiferromagnetic long-range ordered state with unconventional critical exponents. The temperature variation of the  $g$ -factor further confirms the antiferromagnetic phase transition and reflects the underlying magnetocrystalline anisotropy of the compound.

DOI: [10.1103/PhysRevResearch.6.033027](https://doi.org/10.1103/PhysRevResearch.6.033027)

**I. INTRODUCTION:**

Quantum fluctuations arising due to geometrical frustration are currently an intensively studied topic in condensed matter physics. In this respect, antiferromagnetically coupled spin  $S = 1/2$  entities arranged on a two-dimensional (2D) triangular lattice provide the simplest model system, where competing spin-spin exchange pathways may give rise to exotic magnetic ground states. It is now widely accepted, that in zero magnetic field the ground state of a 2D triangular lattice with nearest-neighbor antiferromagnetic interaction is a three-sublattice 120° order [1–8]. However, in real materials due to complex structural arrangements the influence of the magnetic interaction with next-nearest (or still further) neighbors

may be significant. In layered compounds, residual interlayer coupling as well as possible anisotropies of the spin-spin interactions also becomes important. In this direction, substantial theoretical effort to study the antiferromagnetic Heisenberg model with additional terms, such as second-neighbor interactions, ring exchanges etc. are found to give rise to other interesting phases including the Dirac quantum spin liquid [9]. However, due competing phases, despite the relentless efforts of many decades, our understanding of the ground state of a  $S = 1/2$  triangular lattice system is yet incomplete and highly debated.

To this end, an investigation of the magnetic properties of isolated antiferromagnetically coupled trimers of spins arranged in equilateral triangles, i.e. the elementary building block of a frustrated system in 2D should be enlightening. The Hamiltonian for an equilateral trimer spin system is given by ( $\alpha = 1$ ),

$$H = J[\alpha (\mathbf{S}_1 \cdot \mathbf{S}_2 + \mathbf{S}_2 \cdot \mathbf{S}_3) + \mathbf{S}_1 \cdot \mathbf{S}_3], \quad (1)$$

where  $J$  is the antiferromagnetic exchange interaction between three nearest-neighbor Heisenberg spins  $\mathbf{S}_i$  ( $i = 1, 2, 3$ ) (see also Fig. 4) [10].  $\alpha \neq 1$  describes an isosceles triangle.

The ground state of a half-integer spin triangle is non-trivial and frustrated. In the case of  $S = 1/2$  on an equilateral triangle, the lowest energy state is the fourfold degenerate  $S_{\text{total}} = 1/2$ . The ground state is separated from the next

\*Contact author: sudip.pal111@gmail.com

†Contact author: rekre@fkf.mpg.de

‡Contact author: martin.dressel@pi1.physik.uni-stuttgart.de

§Contact author: puphal@fkf.mpg.de

Published by the American Physical Society under the terms of the Creative Commons Attribution 4.0 International license. Further distribution of this work must maintain attribution to the author(s) and the published article's title, journal citation, and DOI. Open access publication funded by Max Planck Society.

excited state of  $S_{\text{total}} = 3/2$  with an energy gap of  $3J/2$ . Quantum spin trimers exhibit varying quantum phases and non-trivial magnetic excitations [11–14].

Trimers might be an important ingredient for various other 2D lattices with subtle distortion, as proposed for the kagome [15], which was discussed in experiments for  $\text{Cu}_3\text{V}_2\text{O}_7(\text{OH})_2 \cdot 2\text{H}_2\text{O}$  [16], but doubts remained as a 1D chain might be better able to describe the experimental picture [17]. Recent structural investigations of low temperature diffraction on various kagome systems show that a structural instability induces distortions in barlowite, claringbullite [18], volborthite [19], and vesignieite [20] making it a typical structural motif at low temperatures, in addition to systems that are already distorted at room temperature such as Y-Kapellasite [21], where theoretical studies show a unique sublattice realization consisting of triangle building blocks [22]. Thus understanding the building blocks of such lattices is essential. Moving to real trimer sublattice systems, realization in inorganic compounds is rare and is usually found as linear trimers as found in 9R-type perovskites like  $\text{Ba}_5\text{Ru}_3\text{O}_{12}$  [23] and its family  $\text{Ba}_4\text{MRu}_3\text{O}_{12}$  [24] or  $\text{Ba}_4\text{Ir}_3\text{O}_{10}$  [12], etc., as well as linear chains that trimerize as in  $\text{Na}_2\text{Cu}_3\text{Ge}_4\text{O}_{12}$  [14].

So far, the best established real isolated  $S = 1/2$  trimer system,  $\text{La}_4\text{Cu}_3\text{MnO}_{12}$ , has been studied using bulk magnetization, specific heat at zero magnetic field, and neutron scattering experiments [25–28].  $\text{La}_4\text{Cu}_3\text{MnO}_{12}$  undergoes antiferromagnetic order below  $T = 2.6$  K, and exhibits a plateau in the magnetization above a critical field of approximately 20 T. However, this compound suffers from disorder that arises from a split Cu site. The scarcity of such compounds, particularly good quality single crystals restricted the experimental realization of further investigations.

Here, we report on the magnetic and magnetothermal properties of the system  $\text{SrCu}(\text{OH})_3\text{Cl}$  which features antiferromagnetically coupled spin  $S = 1/2$  trimers arranged in magnetically isolated isosceles triangles.  $\text{SrCu}(\text{OH})_3\text{Cl}$  has firstly been synthesized and its crystal structure has been determined by Zhu *et al.* [29].  $\text{SrCu}(\text{OH})_3\text{Cl}$  crystallizes in the orthorhombic space group no. 31 containing two different Cu atoms. Of interest for its magnetic properties are three  $\text{Cu}^{2+}$  cations arranged in isosceles triangles which are well separated from each other as displayed in Fig. 1. The two Cu2 atoms are 3.2594(18) Å apart, while their distance to the Cu1 atom is with 3.3948(15) Å slightly elongated. The next-nearest neighbors are with 5.0974(16) and 5.1869(18) Å between the green and blue Cu atoms in chains both along b and c. The  $\text{Cu}^{2+}$  cations each are coordinated by four oxygen atoms at distances of  $\sim 2$  Å forming equatorial planes containing the Cu  $d_{x^2-y^2}$  orbitals. Cl atoms are at apical positions at distances of  $\sim 3.1$  Å. The Cu-O-Cu bonding angles amount to  $119.4^\circ$  ( $2\times$ ) and  $112.6^\circ$  ( $1\times$ ), respectively.

The crystal structure of  $\text{SrCu}(\text{OH})_3\text{Cl}$  has been described as consisting of cuprate layers in the 011 planes with the alternating orientation of the triangular planes, thus being different from the parallel arrays in the kagome layers found in the related copper hydroxy chloride family  $\text{ACu}_3(\text{OH})_6\text{Cl}_2$  [30]. First magnetic characterization by Zhu *et al.* indicated rather sizable exchange interaction between the Cu spins. At high temperatures, the inverse magnetic susceptibility followed a Curie-Weiss behavior with a Curie-Weiss temperature

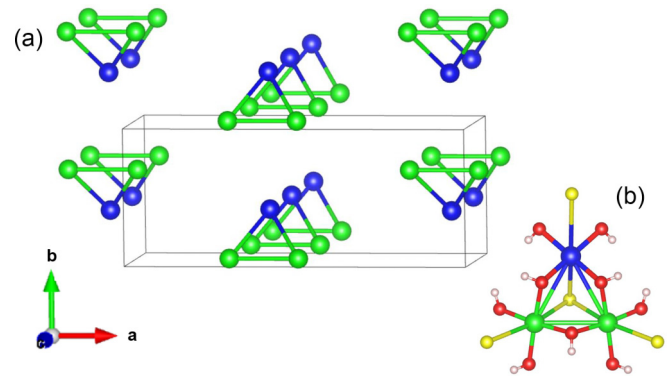


FIG. 1. Crystal structure of  $\text{SrCu}(\text{OH})_3\text{Cl}$ . (a) Arrangement of the Cu isosceles triangles. A unit cell is outlined. (b) Coordination of Cu by oxygen and chlorine atoms. The blue/green, red, yellow spheres represent Cu, O, and Cl atoms, respectively.

of around  $-135$  K, indicating predominant antiferromagnetic exchange between the Cu moments. Magnetization measurements at 2 K proved saturation with a saturated moment of  $\sim 1 \mu_B$  indicating a spin  $S = 1/2$  ground state with a  $g$ -factor close to 2.  $\text{SrCu}(\text{OH})_3\text{Cl}$  bears some similarity to trimer molecular magnets, where isolated magnetic clusters are either a part of a two- or three-dimensional lattice or are surrounded by non-magnetic ligands [31,32].

We have grown high-quality single crystals of  $\text{SrCu}(\text{OH})_3\text{Cl}$  and investigated the magnetic and thermodynamic properties using bulk magnetization, nuclear magnetic resonance (NMR), electron spin resonance (ESR) spectroscopy and specific heat measurements. The temperature-dependent magnetization,  $M(T)$  does not indicate any phase transition down to  $T = 2$  K as reported earlier. However, our specific heat measurements in zero magnetic field reveals a  $\lambda$ -type anomaly at  $T \approx 1.2$  K involving the removal of a magnetic entropy corresponding to a spin  $S = 1/2$  entity. The temperature dependence of the ESR linewidth and of the  $g$ -factor supports this finding. A magnetic phase diagram is constructed from the magnetic field dependence of the specific heat at low temperatures.

## II. EXPERIMENTAL DETAILS

Transparent blue single crystals [see Fig. 2(b)] of  $\text{SrCu}(\text{OH})_3\text{Cl}$  were grown hydrothermally using a hydroflux method which was modified as compared to the description given in Ref. [29]. A mixture of 5.34 g  $\text{SrCl}_2 \cdot 6\text{H}_2\text{O}$ , 2.666 g  $\text{CuCl}_2 \cdot 2\text{H}_2\text{O}$ , 2.4 g LiOH was poured sequentially into a 30 ml Teflon lined autoclave without any further addition of water or stirring and heated with 0.1 K/min to  $240^\circ\text{C}$ , subsequently held and cooled with an oscillatory profile at a rate of 0.1 K/min. The crystals were finally washed with distilled water. The structural properties of the obtained crystals were characterized using powder x-ray diffraction (PXRD) performed at room temperature using a Rigaku Mini-flex diffractometer with Bragg Brentano geometry, Cu  $K_\alpha$  radiation, and a Ni filter. Rietveld profile refinements were conducted with the FullProf software suite [33]. Single crystal diffraction was performed at room temperature using a

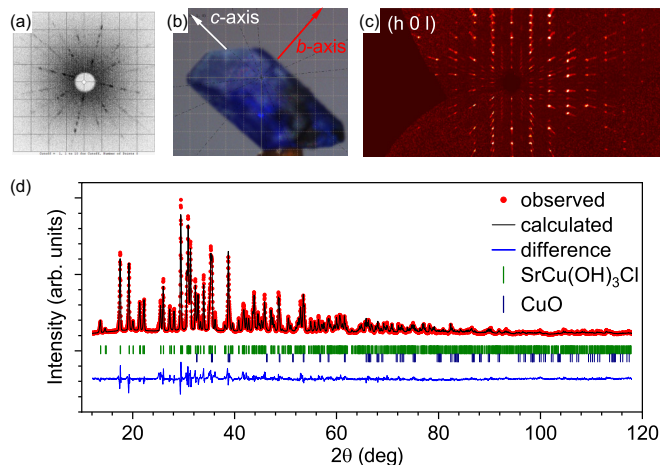


FIG. 2. X-ray diffraction of SrCu(OH)<sub>3</sub>Cl single crystals: (a) Laue diffraction along the  $a$  axis, (b) picture of a single crystal with axis indication, (c) single crystal diffraction map of the  $(h0l)$  plane, and (d) powder diffraction pattern of crushed crystals.

Rigaku XtaLAB mini II with Mo  $K_{\alpha}$  radiation. The data were analyzed with the CrysAlis(Pro) software and the final refinement done using Olex2 with SHELX. The magnetization measurements have been performed at temperatures  $2 \leq T \leq 300$  K using a superconducting quantum interference device (MPMS3, Quantum Design). The specific-heat measurements were carried out, down to  $T = 400$  mK in a Physical Properties Measurement System (PPMS, Quantum Design) equipped with the He3 option. We note here that due to very small mass of the individual crystals, the specific heat measurements have been performed on an assembly of nine single crystals amounting to 1.717 mg oriented with magnetic field aligned along the  $c$ -axis. The  $^1\text{H}$  NMR experiments were performed in a 14 T PPMS (Quantum Design) cryostat at temperatures 3–110 K in an external magnetic field 1.79 T. The spin-lattice relaxation rate  $T_1^{-1}$  was determined nonselectively from stretched exponential fits of the recovery curves with an exponent between 0.8–1.0, i.e., close to single-exponential recovery. The ESR spectra were collected in a Bruker X-band spectrometer ( $\nu = 9.47$  GHz) equipped with a continuous He gas flow cryostat working in the temperature range down to  $T = 1.8$  K. The signal-to-noise ratio of the spectra is improved by recording the field derivative of the absorption spectra ( $dP/dH$ ) using the lock-in technique with field modulation at 100 kHz. The samples were fixed in a quartz tube by paraffin and could be rotated using an automated goniometer.

### III. RESULTS AND DISCUSSIONS

#### A. X-ray diffraction

Crystals were checked with single crystal x-ray diffraction (XRD) and oriented with Laue diffraction for the susceptibility measurements [see Fig. 2(a)]. As reported in Ref. [29] the system crystallizes in  $Pmn2_1$  (space group No. 31). The lattice parameters extracted from the single crystal x-ray diffraction data amount to  $a = 15.984(2)$  Å,  $b = 6.3905(11)$  Å, and  $c = 6.4694(17)$  Å, in agreement with those given by Zhu *et al.* The refined atom positions are compiled in Table I. The powder

TABLE I. Refined atom positional coordinates of SrCu(OH)<sub>3</sub>Cl in the orthorhombic space group  $Pmn2_1$  (No. 31), extracted from single crystal XRD.

Atom	x	y	z	Uiso (Å <sup>2</sup> )	Occ.
Sr1	0.5	0.3352(4)	1.0722(5)	0.0065(6)	1
Sr2	0.17326(9)	0.9289(3)	0.2429(4)	0.0091(5)	1
Cu1	0.39912(13)	0.7980(3)	0.2488(5)	0.0074(6)	1
Cu2	0.5	0.4702(5)	0.5678(7)	0.0071(7)	1
Cl1	0.2636(3)	0.6757(7)	-0.0758(10)	0.0146(11)	1
Cl2	0	1.0588(12)	0.1321(14)	0.0177(17)	1
O1	0.4166(8)	0.516(2)	0.353(2)	0.007(3)	1
O2	0.3842(9)	1.065(2)	0.116(2)	0.009(3)	1
O3	0.3043(9)	0.838(2)	0.431(3)	0.009(3)	1
O4	0.4129(8)	0.394(2)	0.758(3)	0.009(3)	1
O5	0.5	0.747(3)	0.092(3)	0.007(4)	1

diffraction patterns revealed a minute CuO impurity. Some crystals were crushed for powder x-ray diffraction.

#### B. Direct current magnetic measurements

In Fig. 3(a), we show the temperature dependence of the magnetic susceptibility ( $M/H$ ) of SrCu(OH)<sub>3</sub>Cl along the three crystal axes measured in an external field of  $\mu_0 H = 1$  T. The measurements were carried out in the zero field cooled measurement protocol. The susceptibility monotonically increases with decreasing temperature. It does not show any anomaly indicative of a phase transition down to the lowest measured temperature of  $T = 2$  K, which is in accordance with the earlier report by Zhu *et al.* [29]. In the right panel of Fig. 3(a), we plot the temperature variation of the inverse susceptibility,  $\chi^{-1}(T)$  along the crystallographic  $a$  direction in the temperature range between  $T = 2$ –300 K. At higher temperatures,  $\chi^{-1}(T)$  exhibits a linear  $T$  dependence, which changes its slope between  $T = 50$ –80 K and again becomes linear at low temperatures. The susceptibility above  $T \sim 80$  K can be fitted well using the Curie-Weiss law with the Weiss temperature of  $\theta_{\text{CW}} = -143$  K and effective moment of  $\mu_{\text{eff}} = 1.85 \mu_B$  ( $g = 2.18$ ). On the other hand at lower temperatures, the linear fit of  $\chi^{-1}(T)$  yields the Curie-Weiss temperature is  $\theta_{\text{CW}} = 0.04$  K. The Curie-Weiss law at high temperatures proves a rather large intra-trimer antiferromagnetic interaction ( $J \sim 10^2$  K) as already concluded by Zhu *et al.* The inter-trimer antiferromagnetic interaction is extremely small as suggested by the small Curie-Weiss temperature obtained from the data at lower temperatures.

Zhu *et al.* have fitted the full temperature dependence of the magnetic susceptibility to a model assuming identical exchange parameters between the three spin  $S = 1/2$  entities. However, the crystal structure data of SrCu(OH)<sub>3</sub>Cl revealed two different Cu atoms, rather indicating that a description in terms of an isosceles triangle with two identical exchange parameters ( $\alpha J$ ) and one exchange ( $J$ ) may be appropriate to model the full temperature dependence of the magnetic susceptibility (see Fig. 4).

Haraldsen *et al.* have calculated the temperature dependence of the magnetic susceptibility of an isosceles triangle describe by the Hamiltonian given by Eq. (1) [34]. It is



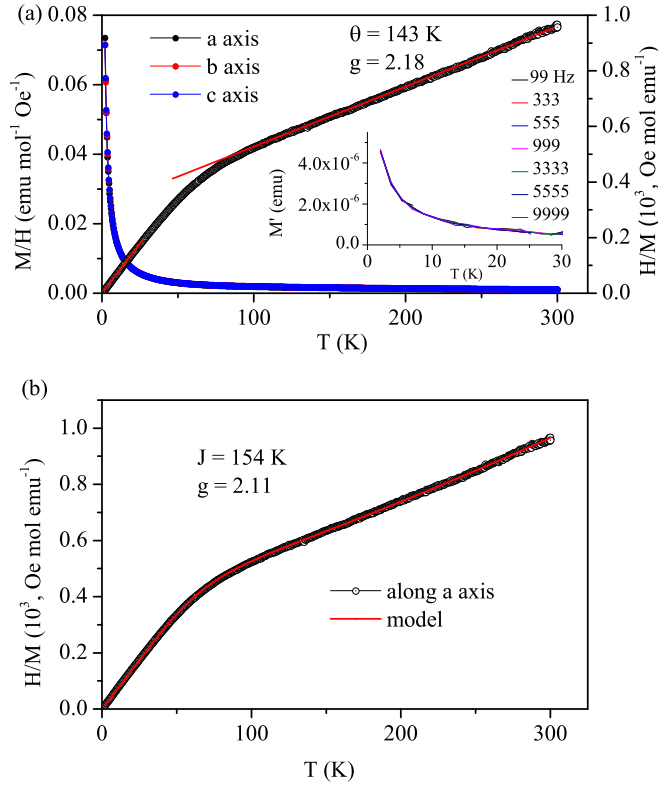


FIG. 3. (a) Temperature dependence of dc magnetic susceptibility along three crystallographic directions measured at  $\mu_0 H = 1$  T (notably the three curves lie nearly indistinguishable atop each other). In the same figure the black points with the right axis give the temperature variation of the inverse susceptibility ( $\chi^{-1} = H/M$ ) along the  $a$ -axis, where the red lines are the Curie-Weiss fits at high and low temperatures. The magnitude of the  $H/M$  is shown on the right axis. Inset shows the frequency dependence of ac susceptibility at low temperatures. (b) shows the fitting of the inverse susceptibility assuming isotropic exchange interaction between spins on an equilateral triangle.

given by

$$\frac{4k_B T \chi}{g^2 \mu_B^2} = \frac{10 + \exp(3\alpha J/2k_B T) + \exp([2 + \alpha] J/2k_B T)}{2 + \exp(3\alpha J/2k_B T) + \exp([2 + \alpha] J/2k_B T)}, \quad (2)$$

which for  $\alpha = 1$  converts to the equation used by Zhu *et al.* to fit their data. Figure 3(b) displays our fit of the magnetic susceptibility measured with magnetic field applied along the  $a$  axis indicating an exchange parameter

$$J = 154 \text{ K.}$$

We note that our value is substantially smaller than that given by Zhu *et al.* ( $233 \text{ cm}^{-1} \approx 335 \text{ K}$ ). Interestingly the fits converge to  $\alpha \approx 1$ , suggesting a symmetric, i.e., equilateral trimer, despite the presence of two different Cu atoms and different bonding distances and Cu-O-Cu bonding angles. Model calculations with  $J = 154 \text{ K}$  and  $\alpha = 1$  yield a Curie-Weiss temperature of  $-133 \text{ K}$ , very close to the result of the Curie-Weiss fit of our high temperature data.

Assuming an additional temperature independent term,  $\chi_0$  due to core diamagnetism and van Vleck contribution, the

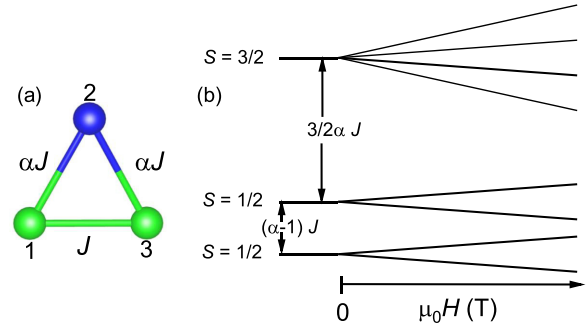


FIG. 4. (a) Definition of the spin exchange parameters.  $\alpha J$  and  $J$ , for the Cu isosceles triangles in  $\text{SrCu}(\text{OH})_3\text{Cl}$ . Blue and green spheres denote the different Cu atom sites. (b) Energy level diagram of the isosceles triangle (not to scale). In case of  $\alpha = 1$  the two doubly degenerate  $S = 1/2$  levels are degenerate.

$\chi^{-1} - T$  curve can be approximated very well by [Eq. (2)]. From the fitting, we obtain  $J = 154 \text{ K}$ , and a  $g$ -factor of  $g = 2.11$  well in line with our experimental determined value of  $2.15(3)$  from ESR and  $\chi_0 = -60 \times 10^{-6} \text{ emu/mole Oe}$ . The diamagnetic contribution estimated for  $\text{SrCu}(\text{OH})_3\text{Cl}$  is  $\chi_{\text{dia}} \sim -90 \times 10^{-6} \text{ emu/mole Oe}$  [35], which gives an approximate estimation of the van Vleck contribution of about  $\chi$  (van-Vleck)  $= 30 \times 10^{-6} \text{ emu/mole Oe}$ . In the inset of Fig. 3(a), we have also shown the temperature dependence of the real part of the ac susceptibility in the low temperature region down to  $T = 1.8 \text{ K}$ . The ac susceptibility monotonically increases with decrease in the temperature and does not exhibit any signature of a phase transition down to  $T = 1.8 \text{ K}$ . Moreover, the ac susceptibility is independent of frequency in the probing frequency range (0.1–10 KHz). This indicates that  $\text{SrCu}(\text{OH})_3\text{Cl}$  is paramagnetic down to  $1.8 \text{ K}$ , which is consistent with the dc susceptibility measurement.

Figure 5 displays the isothermal magnetization collected at  $1.8 \text{ K}$  with the magnetic field aligned along the crystal needle ( $c$  axis). Measurements with  $a$ -axis,  $b$ -axis, and  $c$ -axis orientations are identical within error bars.

In the main panel of the Fig. 5, we show the magnetic field dependence of the dc magnetization (isothermal  $M-H$ ) curves along the three crystal axes at temperature  $T = 1.8 \text{ K}$ . Note that, along all three directions, the  $M-H$  curves reaches a saturation value of the magnetic moment of  $\sim 0.33 \mu_B/\text{Cu}$  atoms, i.e.,  $1/3$  of  $M_s$  per formula unit. The magnetization can be easily fitted with a Brillouin function for  $S = 1/2$  and  $T = 1.8 \text{ K}$ .

At high magnetic fields, the magnetization per Cu trimer saturates to a magnetic moment of  $1/3 \mu_B$  per formula unit. The field dependence follows very well the Brillouin function for one isolated spin  $S = 1/2$  entity, indicating that each Cu triangle is antiferromagnetically coupled and has a ground state of an effective spin  $1/2$  and is magnetically well isolated from its neighboring triangles.

### C. Specific heat measurements

To further investigate the magnetic ground state, we have carried out temperature and magnetic field dependent specific heat measurements of  $\text{SrCu}(\text{OH})_3\text{Cl}$  down to  $400 \text{ mK}$ . The

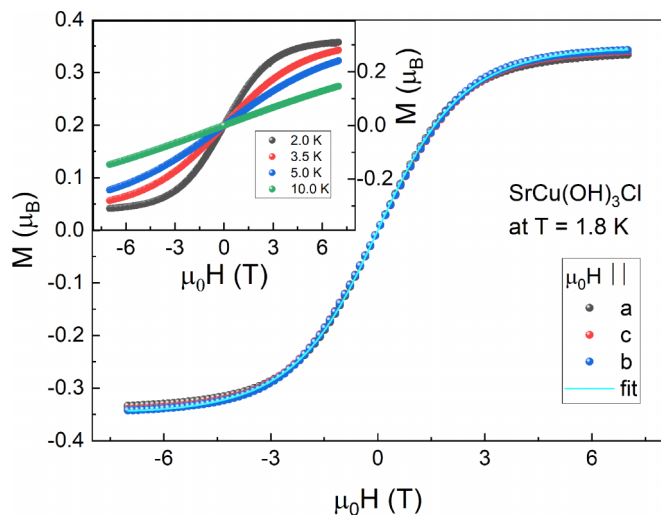


FIG. 5. The main panel shows the magnetization versus field applied along all three crystallographic directions at 1.8 K. The solid bright blue line represents a fit with a Brillouin function for  $S = 1/2$  and  $g = 2.11$ . The inset displays the isothermal magnetization curves for various temperatures.

total specific heat as a function of temperature at  $H = 0$  is plotted in Fig. 6(a). The zero-field specific heat shows a  $\lambda$ -type anomaly at  $T = 1.2$  K, and a weak broad hump-like feature at higher temperatures centered around  $T = 1.9$  K. The  $\lambda$ -type feature proves that the system undergoes a second order phase transition below  $T_N = 1.2$  K, apparently of magnetic origin due to some very weak exchange interaction between the “compound” spins of the Cu triangles. We highlight that a broad shoulder starts significantly above the  $\lambda$  (below  $\sim 3$  K) anomaly, which can be ascribed to short range spin correlations preceding the long range magnetic order at  $T_N$ .

To obtain the magnetic heat capacity contribution we subtracted a phonon part from the total heat capacities. The phonon contribution shown by the solid red line in Fig. 6(a) was determined by fitting a  $T^3$  power law to the heat capacities in the temperature range between  $\sim 4.5$ – $20$  K and extrapolating it to  $T \rightarrow 0$  K. The magnetic entropy displayed in Fig. 6(b) was calculated by integrating the magnetic heat capacity,  $\int (C_m/T) dT$ . It saturates to a value very close to  $\frac{1}{3}R\ln(2)$ , where  $R$  is the molar gas constant. The  $S_{\text{total}} = 1/2$  ground state of an equilateral triangle cluster is fourfold degenerate. A complete lifting of the degeneracy, e.g., by a small asymmetry of the triangle exchange (i.e.,  $\alpha \neq 1$ ) and an inter trimer exchange interaction the entropy would add up to  $2R \ln(2)$ . For  $\alpha = 1$ , however, the entropy remains at  $R\ln(2)$ , since the  $S_{\text{total}} = 1/2$  degeneracy is not lifted and the ground state splits into two states, each with twofold degeneracy [34]. In addition to the magnetic susceptibility and the isothermal magnetization measurements that found saturation at a value of  $\sim 1 \mu_B$  per Cu triangle, the magnetic entropy therefore also supports  $\alpha = 1$ , i.e., a ‘magnetically symmetric’ equilateral triangle despite the structural asymmetry. In Fig. 7, we show the effect of an external field on the specific heat. A rather small external magnetic field of 1 T is sufficient to suppress the antiferromagnetic transition,  $T_N$  down to  $T \sim 0.8$  K, which is nearly half of the  $T_N$  at zero field.

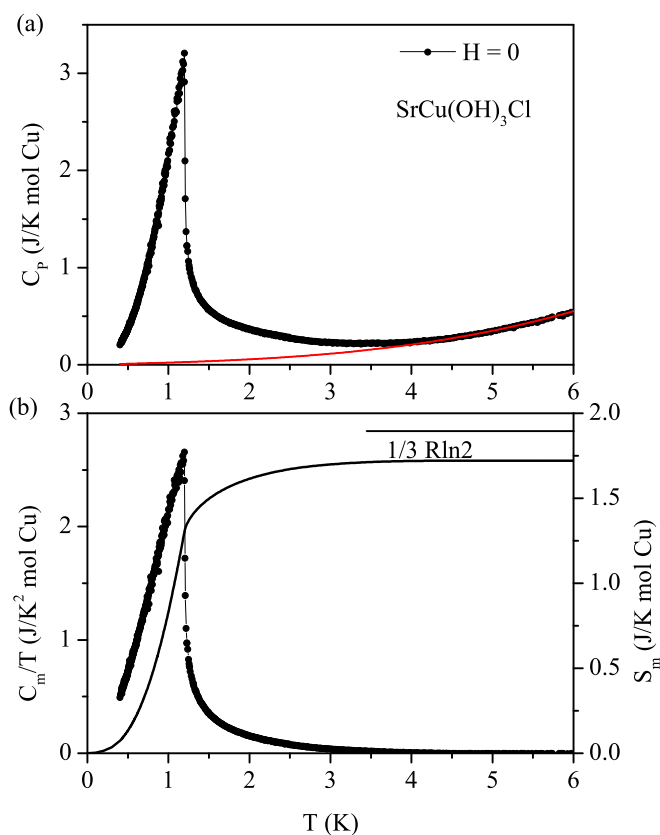


FIG. 6. (a) Temperature dependence of the total specific heat at  $H = 0$ . It reveals a  $\lambda$  anomaly at  $T_N = 1.2$  K. The red line gives the approximation from its phonon contribution to the heat capacity. (b) Temperature dependence of  $C_m/T$ , across  $T_N$ , where  $C_m$  is the magnetic heat capacity. The right panel displays the magnetic entropy released across the transition.

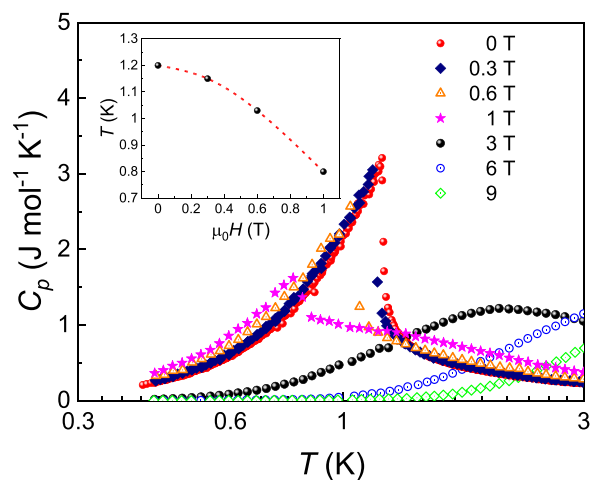


FIG. 7. Magnetic field dependence of the specific heat of SrCu(OH)<sub>3</sub>Cl applied along the  $a$ -direction. The  $\lambda$  anomaly associated with antiferromagnetic transition is gradually suppressed with increasing magnetic field (see the inset). At higher field an additional broad anomaly appears which shifts to higher temperatures with field.

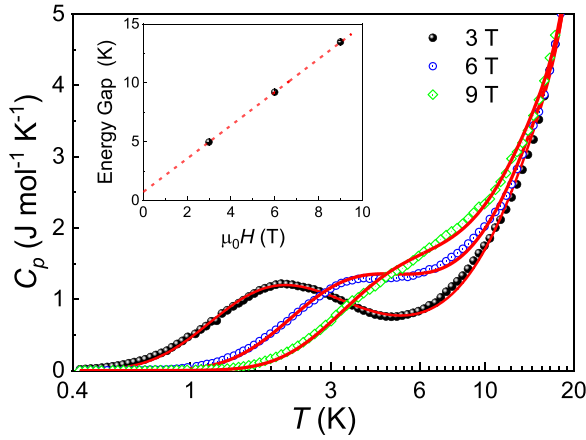


FIG. 8. Specific heat curves of  $\text{SrCu}(\text{OH})_3\text{Cl}$  measured in magnetic fields starting from 3 T. The (red) solid lines are fits with the heat capacity expected for a two-level system including a phonon term as described in detail in the text. The inset displays the level-splitting as a function of the magnetic field.

The rapid suppression of the  $T_N$  by small magnetic field is consistent with the weak intertrimer exchange interaction. In the inset of Fig. 7, we show the variation of  $T_N$  with magnetic field up to 1 tesla. Extrapolating our dataset we assume a full suppression at 1.33 T. At higher fields, we observe a broad anomaly which starts to shift towards higher temperatures with increasing fields, which coincides with 1/3 saturation observed in magnetization measurements at 1.8 K shown in Fig. 5.

The broad heat capacity anomaly appearing at higher magnetic fields can be successfully fitted by assuming a two-level Schottky system with an energy gap  $\Delta$  and a degeneracy of two for each level. The red solid lines in Fig. 8 displays the heat capacities fitted to a system using Eq. (3) including a phonon contribution. Our fits yield a uniform Debye temperature of 200(3) K.

$$C_p = R \frac{1}{3} \frac{g_1}{g_2} (\Delta/k_B T)^2 e^{\Delta/k_B T} / (1 + e^{\Delta/k_B T})^2 + C_{\text{phon}}, \quad (3)$$

$g_1$  and  $g_2$  are the degeneracies of the two levels for the phonon heat capacity contribution,  $C_{\text{phon}}$ , we used a polynomial description according to

$$C_{\text{phon}} = \beta T^3 + \gamma T^5 + \delta T^7. \quad (4)$$

The energy difference  $\Delta$  of the two levels increases linearly with magnetic field as shown in detail in the inset in Fig. 8 with an intersection of 0.73 K for vanishing magnetic field, indicating an internal exchange field of  $\sim 1$  T causing the long-range antiferromagnetic ordering at 1.2 K.

#### D. Nuclear magnetic resonance

Temperature dependent  $^1\text{H}$  NMR was used to probe the paramagnetic state of  $\text{SrCu}(\text{OH})_3\text{Cl}$ . The NMR spectrum collected at 3 K in an external magnetic field of 1.79 T, shown in Fig. 9(a), consists of two resonance lines at 76.12 and 76.18 MHz with FWHM of  $\sim 40$  kHz. The intensity ratio of the two resonance lines amounts to  $\sim 3 : 2$ , reflecting the

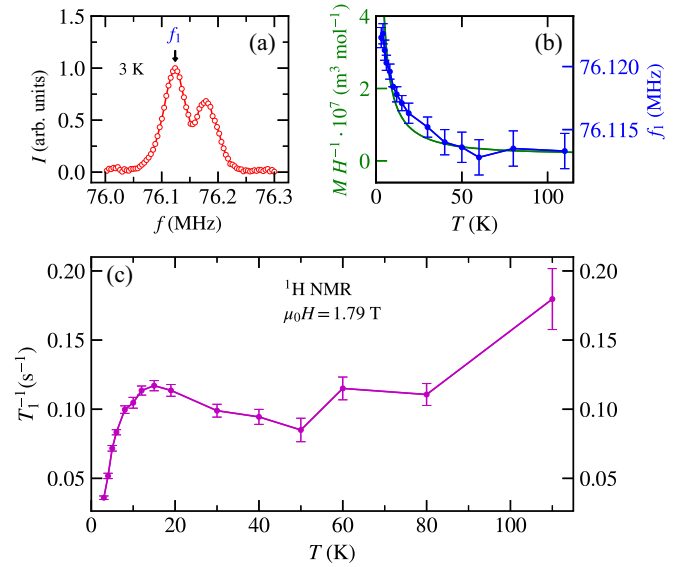


FIG. 9. (a) The  $^1\text{H}$  NMR spectrum of  $\text{SrCu}(\text{OH})_3\text{Cl}$  at 3 K exhibits similar line splitting into two peaks as related single-crystalline  $\text{Cu}^{2+}$  hydroxide systems in the paramagnetic state [36]. (b) The frequency shift of resonance line  $f_1$ , marked by the arrow in (a), follows a similar temperature dependence as the magnetic susceptibility. (c) Temperature-dependent spin-lattice relaxation rate probed by  $^1\text{H}$  NMR.

five inequivalent proton positions in the crystal structure of  $\text{SrCu}(\text{OH})_3\text{Cl}$  [29]. The coupling between magnetic properties and NMR spectrum is well visible from Fig. 9(b), which compares the magnetic susceptibility with the frequency shift of the  $f_1$  peak at 76.12 MHz.

The temperature-dependent spin-lattice relaxation rate,  $T_1^{-1}$  shown in Fig. 9(c), of the protons in the hydroxyl groups was analyzed to probe the paramagnetic state and the magnetic fluctuations above the magnetic ordering. Below 100 K,  $T_1^{-1}$  decreases upon cooling and exhibits a local minimum around  $\sim 50$  K, which coincides with the change in slope of inverse susceptibility in Fig. 3 that was discussed above in the context of the thermal population of isolated spin trimers on the  $\text{Cu}^{2+}$  triangles. At lower temperatures,  $T_1^{-1}$  develops a broad maximum at around 15 K, below which the relaxation rate drops rapidly. Commonly, a strong increase of  $T_1^{-1}$  due to spin fluctuations is expected upon antiferromagnetic ordering, which results in a peak in  $T_1^{-1}$  as observed in other Cu-based hydroxide systems [36]. In the present case, however, the rapid reduction of relaxation rate below 10 K and the lack of experimental data below 3 K precludes the observation of a peak in  $T_1^{-1}$ . A closer look at Fig. 7 suggests that antiferromagnetism may indeed be fully suppressed at the magnetic field (1.79 T) applied for NMR investigations. Instead, the drop of  $T_1^{-1}$  may be related to the field-dependent energy gap formation in Fig. 8.

#### E. Electron spin resonance

In Fig. 10, we show representative ESR spectra along the three crystal axes recorded at  $T = 1.8$  K. Notably, the lowest stable temperature we achieve in our set up is  $T \sim 1.8$  K, well above the onset of long range antiferromagnetic order at

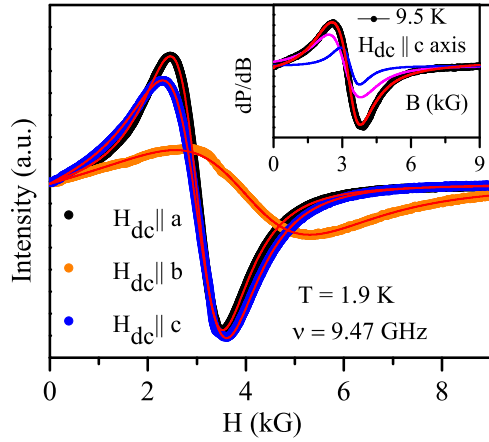


FIG. 10. The main panel shows the ESR resonance of SrCu(OH)<sub>3</sub>Cl along the three crystal axes at  $T = 1.8$  K. The red lines are fits of the ESR lines using Eq. (5). (Inset) The fitting of the ESR line recorded at  $T = 9.5$  K along  $H_{dc} || c$  axis using two Lorentzian lines as described in detail in the text.

$T_N \sim 1.2$  K for SrCu(OH)<sub>3</sub>Cl. Moreover, as the temperature increases, the ESR signal becomes broader and the intensity reduces dramatically, which make it difficult to reliably record any ESR signal above  $T = 35$  K. The ESR spectra shown in the main panel of Fig. 10 indicates that the ESR resonance field along  $H_{dc} || b$  axis is much larger than a and c-axis at  $T = 1.8$  K. In all directions, the ESR spectra are well described by the field derivative of a single Dysonian line. Since the ESR line width is large and of the same order of magnitude as the resonance field, we have to incorporate the contributions from both the right circular and left circularly polarized components contained in the linearly polarized microwave excitation [37,38]. Hence, the resonance at the reversed magnetic field  $-H_0$  has to be included into the fitting equation, which is then given by

$$\frac{dP}{dH} \propto \frac{d}{dH} \left[ \frac{W + \sigma(H - H_0)}{H_0^2 + (H - H_0)^2} + \frac{W + \sigma(H + H_0)}{H_0^2 + (H + H_0)^2} \right]. \quad (5)$$

Here,  $H_0$  and  $W$  are the resonance field and the linewidth, respectively. The parameter  $\sigma$  in Eq. (5) denotes the dispersion-to-absorption ratio, which describes the asymmetry of the ESR line shape. Such asymmetric ESR lines are generally observed in metallic samples where the skin effect due to large conductivity of the material causes the electric and magnetic fields of the microwave out of phase [39]. Therefore an asymmetric ESR line shape is *per se* not expected in an insulating compound like SrCu(OH)<sub>3</sub>Cl. In case of low-dimensional spin systems, a finite  $\sigma$  may arise in magnetic insulators due to admixture of nondiagonal elements of the dynamic susceptibility to the signal, which distorts the ESR signal with a large value of the linewidth [40]. Such a behavior has been observed in one-dimensional spin chain compounds with strong spin-orbit coupling [40,41]. Moreover, in these systems the ESR spectra is symmetric at high temperatures and the distortion parameter,  $\sigma$  gradually increases as the system approaches  $T_N$  from the high temperatures side. As we will discuss later, the temperature variation of  $\sigma$  in SrCu(OH)<sub>3</sub>Cl is more complex. One possibility of such asymmetric ESR

absorption might be a convolution of multiple ESR absorption lines. In SrCu(OH)<sub>3</sub>Cl, there are two in-equivalent Cu atoms within a spin-trimer. In the inset of Fig. 10, we show the modeling of the ESR line at  $T = 9.5$  K measured along  $H_{dc} || c$  axis assuming two Lorentzian lines with 2:1 intensity ratio and  $g = 2.15(3)$  and  $2.02(3)$  and linewidths of 1275(30) and 692(20) G. However, due to large linewidth, and absence of clear splitting between the two resonance lines, the significance of such fits is limited. In this context, it may also be mentioned that the ESR spectra of finite size systems such as XXZ spin chain with finite lengths or molecular magnets shows a double-peak structure at high temperatures which strongly differs from usual Lorentzian line shape [42]. The separation of the peaks of the double-peak structure also vanishes inversely with the system size [43]. Therefore the origin of the asymmetry in the present system is not clear.

Nonetheless, to further understand the ESR properties of SrCu(OH)<sub>3</sub>Cl, we have fitted the spectra measured along all three directions using Eq. (5) (see in Fig. 10). The ESR intensity,  $I_{ESR}$  which is obtained by the double integration of the ESR spectra is shown in Fig. 11(a). Consistent with the dc magnetization measurements, the intensity  $I_{ESR}$  along all three direction monotonically increases with decreasing temperature. The intensity does not exhibit any signature of spin freezing or phase transition down to  $T = 1.8$  K. In the inset of Fig. 11(a), we have compared the dc susceptibility ( $\chi_{dc}$ ) with the ESR intensity ( $I_{ESR}$ ) below  $T = 35$  K along the crystallographic  $a$  axis. To compare the intensity  $I_{ESR}$  with  $\chi_{dc}$ ,  $I_{ESR}$  has been normalised to the dc susceptibility data at  $T = 35$  K.

### 1. Critical-point anomalies in ESR linewidth

In Fig. 11(b), we show the temperature variation of the ESR linewidth determined with the magnetic field aligned parallel to the crystallographic  $a$ ,  $b$ , and  $c$  axes. As the temperature is reduced, the linewidth initially decreases, passes through a shallow minimum in the temperature range between  $T = 4$ – $10$  K, and then increases rapidly on approaching  $T_N$ . Particularly, the linewidth along  $H_{dc} || b$  axis is much larger compared to  $H_{dc} || a$  and the  $c$  axes. Moreover, at low temperatures the linewidth exhibits a stronger divergence along  $b$ -axis, as will be discussed later. At high temperatures the temperature dependence of the linewidth along all three crystal directions can be fitted well using the following empirical equation [44]:

$$\Delta H = \Delta H_{\infty} + \Delta H_{act} \exp(-E_g/T). \quad (6)$$

Here,  $\Delta H_{\infty}$  denotes the high-temperature asymptotic contribution due to pure spin-spin relaxation, and the last term describes a thermally activated contribution  $\Delta H_{act}$  characterized by an energy gap  $E_g$ . The values of  $\Delta H_{act}$  and the energy gap  $E_g$  along three directions considering both of them as free parameters are listed in the Table II.

The linewidth ( $\Delta H$ ) of the ESR spectra has proved to be very useful to study the spin dynamics at low temperatures due to dominant spin-spin interaction. In a magnetic crystal each spin is surrounded by a number of other spins at varying distances. Then the interaction between each spin-pairs is a function of distance between them and angle which the line



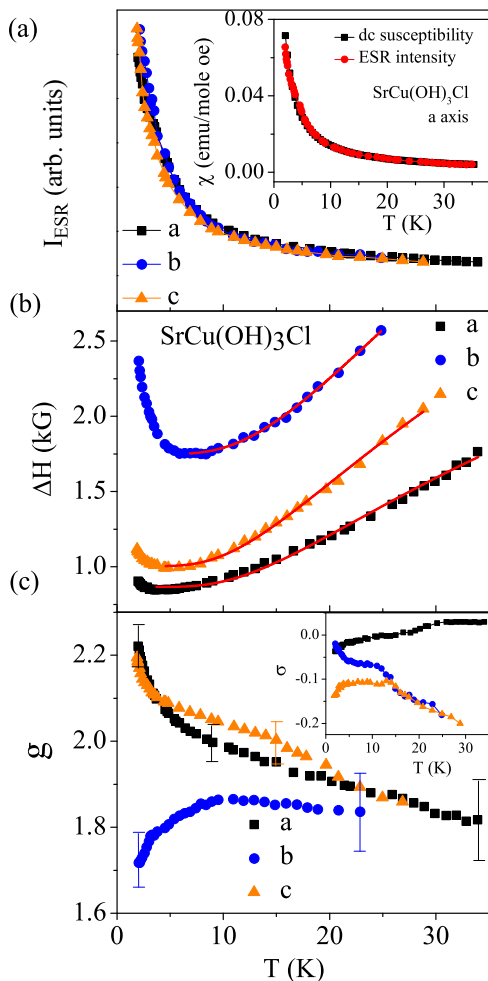


FIG. 11. Temperature dependence of ESR parameters of  $\text{SrCu}(\text{OH})_3\text{Cl}$ . (a) The main panel shows the total intensity of the ESR signal along three different crystallographic directions. (Inset) Comparison of the dc susceptibility measured in a SQUID magnetometer and the ESR intensity. (b) the temperature variation of ESR line width along three directions. The red lines correspond to the fits to the high temperature region using Eq. (6). (c) The main panel shows the temperature variation of the apparent  $g$ -factor obtained from the ESR absorption. (Inset) variation of the dispersion parameter,  $\sigma$  in Eq. (5) as a function of temperature.

joining their centres makes with the crystallographic axes. The ESR  $\Delta H$  depends on the relaxation rate of spin-spin interaction. The divergence of the spin-spin correlations both in time and space in the proximity of the phase transition should be reflected in the temperature and angular dependence of  $\Delta H$  near  $T_N$ . In an antiferromagnetic material, when lowering the temperature towards the phase transition from above, the EPR linewidth becomes critically enhanced by the anomalous

TABLE II. Parameters for ESR linewidth.

Directions	$a$	$b$	$c$
$\Delta H_{\text{act}}$ (kG)	2.7	6.0	4.2
$E_g$ (K)	40.3	48.5	41

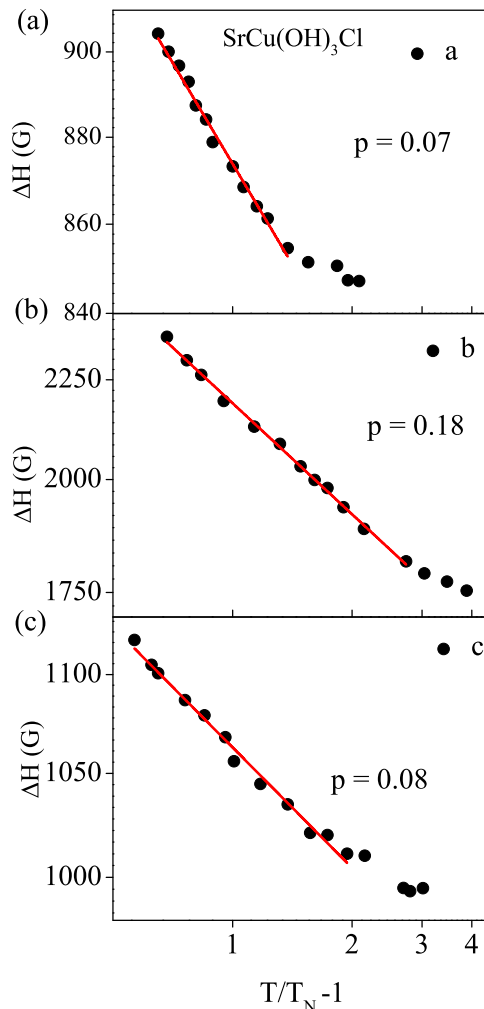


FIG. 12. Double logarithmic plot of  $\Delta H$  and  $(T/T_N - 1)$  on approaching  $T_N = 1.2$  K from  $T > T_N$  along the three crystallographic directions.  $T_N$  is obtained from the specific heat measurements at  $H = 0$ . The red lines show the linear fit to the data points. The slopes of the linear fit, which gives the exponent are also mentioned.

spin-spin relaxation [45–47]. In case of  $\text{SrCu}(\text{OH})_3\text{Cl}$  we observed that at lower temperatures, the linewidth increases down to the lowest measured temperature of  $T = 1.8$  K. It may be noted that in case of the  $\text{SrCu}(\text{OH})_3\text{Cl}$ , such broadening emerges below  $T \sim 3, 4,$  and  $3$  K along  $a, b,$  and  $c$  directions, respectively. Therefore the broadening of the linewidth starts at pretty high temperatures close to around  $3T_N$ , which indicates extended range of short range correlation above  $T_N$ . Such short-range correlations are characteristic features of the frustrated and low-dimension systems, which are more pronounced when the spin value  $S$  is small [48]. This is in line with the appearance of the broad shoulder in specific heat below  $T \sim 3$  K along  $c$  axis above  $T_N$  even at zero magnetic field [Fig. 6(b)]. It is interesting that, the temperature dependent linewidth can be modeled by a power law at low temperatures given by  $(\frac{T}{T_N} - 1)^{-p}$ , where  $T_N$  is the transition temperature, and the exponent  $p$  defines the critical behavior [44]. In Figs. 12(a)–12(c), we show  $\Delta H$  as a function of  $(\frac{T}{T_N} - 1)$  in a log-log scale, which is linear. It indicates

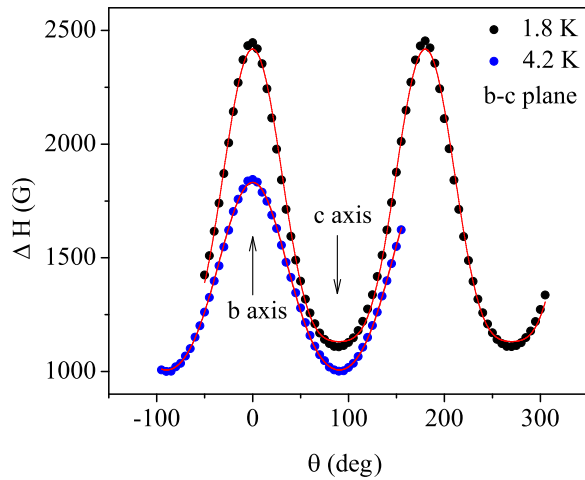


FIG. 13. Angle dependence of the linewidth in the  $b$ - $c$  plane at  $T = 1.8$  and  $4.2$  K. The red line is the fitting of the data as described in detail in the text.

that  $\Delta H$  exhibits power law divergence approximately below  $2.4T_N$ ,  $3.6T_N$ , and  $3T_N$  along  $a$ ,  $b$ , and  $c$  axes with an exponents of 0.07, 0.18, and 0.08, respectively. One possible origin of such a divergence of the linewidth as the  $T_N$  is approached can be due to dominating spin fluctuation near the critical region. Critical linewidth broadening on approaching the antiferromagnetic transition indicates the importance of the increasing critical fluctuation close to antiferromagnetic phase transition, and is a characteristic feature of a second order phase transition. However, we note here that the values of the exponents obtained are significantly smaller compared to other systems with antiferromagnetic long range order. For instance, in a classical uniaxial antiferromagnet  $\text{MnF}_2$ , the linewidth exhibits critical broadening with a critical exponent  $p \sim 1.2$  [47]. However, as mentioned before, in low dimensional systems the short-range spin-spin correlation is dominant and hence may affect the critical behavior. On the other hand, it is also important to note that our ESR measurements are limited to  $T = 1.8$  K, which is much above the transition temperature  $T_N \sim 1.2$  K of  $\text{SrCu}(\text{OH})_3\text{Cl}$ . Therefore its necessary to probe the temperature dependence of the linewidth at further lower temperatures.

It is interesting that the angular dependence of the linewidth is also temperature dependent. In Fig. 13, we show the angular variation of the ESR linewidth in the  $b$ - $c$  plane at  $T = 1.8$  and  $4.2$  K. Note that the angular variation of the linewidth at  $\theta = 0^\circ$  (which corresponds to the applied field is parallel to the crystallographic  $b$  axis) is sharper at lower temperature. At  $T = 4.2$  K, the angle dependence of the linewidth reveals a  $(\cos^2 \theta + 1)$  dependence of the angle,  $\theta$  is the angle between the direction of the static magnetic field and the crystalline axes. As the temperature approaches  $T_N$ , this term alone is not sufficient to describe the angular variation of the linewidth. At  $T = 1.8$  K, an additional term given by  $(3 \cos^2 \theta - 1)^2$  [49] gives satisfactory fit as shown in Fig. 13. The angular dependence of the linewidth showing  $(\cos^2 \theta + 1)$  behavior is regularly encountered in weakly correlated or three-dimensional exchange narrowed spin systems. The additional contribution at  $T = 1.8$  K may be associated

with an additional broadening due to critical fluctuation close to the antiferromagnetic transition. In the case of 2D spin system, such an angular variation of the linewidth has been observed, which is caused by the increasing dominance of the long-wavelength fluctuations in low dimensional magnets [50,51]. Therefore it may be a possible indication of a dimensional crossover from zero dimensional system at high temperatures to a higher dimensional spin system at low temperatures as  $\text{SrCu}(\text{OH})_3\text{Cl}$  undergoes a phase transition below  $T_N$  from an isolated triangular spin system.

## 2. $g$ -factor anomaly

As mentioned before, the unusual asymmetric shape of the ESR spectra in X-band frequency gives rise to large uncertainties in the ESR parameters, including the  $g$ -factor. The magnitude and the temperature dependence of the distortion parameter  $\sigma$  are quite distinct along the three directions, as shown in the inset of Fig. 11(c). In the investigated temperature range, the magnitude of  $\sigma$  is large along  $b$  and  $c$  directions compared to the  $a$  axis. Interestingly, in the temperature variation of  $\sigma$ , we can distinguish three temperature regions, where  $\sigma$  shows different temperature dependence. At low temperatures,  $\sigma$  changes rapidly with increase in the temperatures until  $T = 3$ – $5$  K, which is followed by a plateau region in between  $5$ – $10$  K, followed by rapid change again on further increase in temperature. Such behavior is prominently observed particularly along  $H_{dc} \parallel b$  and  $c$  axis, whereas it is less pronounced for  $H_{dc} \parallel a$ .

Nevertheless, in the main panel of Fig. 11(c), we have shown the temperature variation of the apparent  $g$ -factor obtained from resonance field ( $H_0$ ) and microwave frequency ( $\nu$ ) via the Larmor condition  $h\nu = g\mu_B H_0$ , where  $\nu = 9.47$  GHz is the microwave frequency, and  $H_0$  is obtained from the fitting of the ESR spectra using Eq. (5). The apparent  $g$ -factor along all three directions also exhibits anomalous temperature dependence. At high temperatures,  $g$ -factor is nearly insensitive to the temperature, however, at low temperatures it changes rapidly as the  $T_N$  is approached. It is important to note that the uncertainty of the  $g$ -value becomes larger as the linewidth becomes comparable to the resonance field of the ESR spectra. Therefore one has to consider the strong increase of the linewidth with temperatures. For that reason, we assume the uncertainty in the resonance field as 5% of the line width and obtain the error bars shown in Fig. 11(c) [52]. To further understand the spin dynamics detail ESR measurements at higher frequencies are required.

## IV. SUMMARY

We have studied the magnetic and thermodynamic properties of the single crystalline samples of the quantum spin trimer compound  $\text{SrCu}(\text{OH})_3\text{Cl}$  using ac and dc magnetic susceptibility, specific heat, NMR, and X-band ESR measurements. While the dc magnetic measurement does not show any phase transition down to 2 K, the specific heat measurement exhibit  $\lambda$ -like sharp anomaly at  $T_N = 1.2$  K at zero magnetic field. The anomaly is progressively suppressed at higher fields until it vanishes completely for  $B \geq 3$  T. This indicates that the present compound undergoes an

antiferromagnetic transition at low temperatures. At higher fields, additional features appear in the specific heat, and we have constructed a corresponding  $H$ - $T$  phase diagram. We can describe the temperature dependent magnetization, the field dependent magnetization and the high field specific heat uniquely well with an ideal equilateral isolated triangle simulation, despite the observation that two different Cu atoms are present in the triangles. We have further characterized the magnetic properties by  $^1\text{H}$  NMR and electron spin resonance measurements.  $T_1^{-1}$  probed at 1.79 T exhibits a sharp reduction below  $T \sim 15$  K, which is in line with the suppression of antiferromagnetic order upon application of a moderate magnetic field between 1–3 T, while the NMR spectra agree with the paramagnetic properties. The ESR intensity probed at smaller fields (0.3 T) does not reveal any signature of nearby phase transition, however, the ESR line width rapidly increases at low temperatures which indicates the important role of the critical spin fluctuations above  $T_N$ . Overall this study proves  $\text{SrCu}(\text{OH})_3\text{Cl}$  to be an ideal model system of isolated isosceles triangles in the range of 2–300 K, well captured by theoretical modeling. The different techniques

provide a uniform picture as ESR provides the  $g$ -factor, which matches to our fits of susceptibility, providing precise exchange interactions from a good model fit. The frequency shift of  $^1\text{H}$  NMR agrees with susceptibility. The magnetization reveals a saturation field above 2 T leading to 1/3 magnetization, exactly where we see a gap opening in specific heat, allowing us to estimate its energy. This could help for less directly interpreted techniques such as thermal transport and ultrasound to test their physical understanding in the near future.

## ACKNOWLEDGMENTS

This work was supported by the Deutsche Forschungsgemeinschaft (DFG). We acknowledge support by the DR228/68-1. We also are indebted to G. Unteiner and E. Brücher for their technical assistance and M. Isobe for the use of the Rigaku XRD. Work of P.D. at TU Wien was funded by the Czech Science Foundation (research project GAČR 23-068100). S.B. thanks the CNRS research infrastructure INFRANALYTICS (FR 2054) for support.

- 
- [1] P. Anderson, Resonating valence bonds: A new kind of insulator? *Mater. Res. Bull.* **8**, 153 (1973).
- [2] P. Fazekas and P. W. Anderson, On the ground state properties of the anisotropic triangular antiferromagnet, *Philos. Mag.* **30**, 423 (1974).
- [3] D. A. Huse and V. Elser, Simple variational wave functions for two-dimensional Heisenberg spin- $\frac{1}{2}$  antiferromagnets, *Phys. Rev. Lett.* **60**, 2531 (1988).
- [4] R. R. P. Singh and D. A. Huse, Three-sublattice order in triangular- and Kagomé-lattice spin-half antiferromagnets, *Phys. Rev. Lett.* **68**, 1766 (1992).
- [5] S. Sachdev, Kagomé- and triangular-lattice Heisenberg antiferromagnets: Ordering from quantum fluctuations and quantum-disordered ground states with unconfined bosonic spinons, *Phys. Rev. B* **45**, 12377 (1992).
- [6] A. Szasz, J. Motruk, M. P. Zaletel, and J. E. Moore, Chiral spin liquid phase of the triangular lattice Hubbard model: A density matrix renormalization group study, *Phys. Rev. X* **10**, 021042 (2020).
- [7] T. Jolicoeur and J. C. Le Guillou, Spin-wave results for the triangular Heisenberg antiferromagnet, *Phys. Rev. B* **40**, 2727 (1989).
- [8] T. Susuki, N. Kurita, T. Tanaka, H. Nojiri, A. Matsuo, K. Kindo, and H. Tanaka, Magnetization process and collective excitations in the  $s = 1/2$  triangular-lattice Heisenberg antiferromagnet  $\text{Ba}_3\text{CoSb}_2\text{O}_9$ , *Phys. Rev. Lett.* **110**, 267201 (2013).
- [9] S. Hu, W. Zhu, S. Eggert, and Y.-C. He, Dirac spin liquid on the spin-1/2 triangular Heisenberg antiferromagnet, *Phys. Rev. Lett.* **123**, 207203 (2019).
- [10] O. Kahn, Competing spin interactions and degenerate frustration for discrete molecular species, *Chem. Phys. Lett.* **265**, 109 (1997).
- [11] O. Waldmann,  $Q$  dependence of the inelastic neutron scattering cross section for molecular spin clusters with high molecular symmetry, *Phys. Rev. B* **68**, 174406 (2003).
- [12] G. Cao, H. Zheng, H. Zhao, Y. Ni, C. A. Pocs, Y. Zhang, F. Ye, C. Hoffmann, X. Wang, M. Lee, M. Hermele, and I. Kimchi, Quantum liquid from strange frustration in the trimer magnet  $\text{Ba}_4\text{Ir}_3\text{O}_{10}$ , *npj Quantum Mater.* **5**, 26 (2020).
- [13] N. van Well, M. Bolte, C. Eisele, L. Keller, J. Schefer, and S. van Smaalen, Mixed system  $\text{Cs}_3\text{Cu}_3\text{Cl}_{8-x}\text{Br}_x\text{OH}$  with weakly connected cu-triangles, *J. Phys. Chem. Solids* **140**, 109386 (2020).
- [14] A. K. Bera, S. M. Yusuf, S. K. Saha, M. Kumar, D. Voneshen, Y. Skourski, and S. A. Zvyagin, Emergent many-body composite excitations of interacting spin-1/2 trimers, *Nat. Commun.* **13**, 6888 (2022).
- [15] A. B. Harris and T. Yildirim, Spin dynamics of trimers on a distorted kagome lattice, *Phys. Rev. B* **88**, 014411 (2013).
- [16] O. Janson, S. Furukawa, T. Momoi, P. Sindzingre, J. Richter, and K. Held, Magnetic behavior of volborthite  $\text{Cu}_3\text{V}_2\text{O}_7(\text{OH})_2 \cdot 2\text{H}_2\text{O}$  determined by coupled trimers rather than frustrated chains, *Phys. Rev. Lett.* **117**, 037206 (2016).
- [17] M.-H. Whangbo, H.-J. Koo, E. Brücher, P. Pupal, and R. K. Kremer, Absence of spin frustration in the kagomé layers of  $\text{Cu}^{2+}$  ions in volborthite  $\text{Cu}_3\text{V}_2\text{O}_7(\text{OH})_2 \cdot 2\text{H}_2\text{O}$  and observation of the suppression and re-entrance of specific heat anomalies in volborthite under an external magnetic field, *Condensed Matter* **7**, 24 (2022).
- [18] A. Henderson, L. Dong, S. Biswas, H. I. Revell, Y. Xin, R. Valenti, J. A. Schlueter, and T. Siegrist, Order-disorder transition in the  $S = \frac{1}{2}$  kagome antiferromagnets claringbullite and barlowite, *Chem. Commun.* **55**, 11587 (2019).
- [19] H. Ishikawa, M. Yoshida, K. Nawa, M. Jeong, S. Krämer, M. Horvatić, C. Berthier, M. Takigawa, M. Akaki, A. Miyake, M. Tokunaga, K. Kindo, J. Yamaura, Y. Okamoto, and Z. Hiroi, One-third magnetization plateau with a preceding novel phase in volborthite, *Phys. Rev. Lett.* **114**, 227202 (2015).

- [20] D. Boldrin, K. Knight, and A. S. Wills, Orbital frustration in the  $s = \frac{1}{2}$  kagome magnet vesignieite, BaCu<sub>3</sub>V<sub>2</sub>O<sub>8</sub>(OH)<sub>2</sub>, *J. Mater. Chem. C* **4**, 10315 (2016).
- [21] P. Puphal, M. Bolte, D. Sheptyakov, A. Pustogow, K. Kliemt, M. Dressel, M. Baenitz, and C. Krellner, Strong magnetic frustration in Y<sub>3</sub>Cu<sub>9</sub>(OH)<sub>19</sub>Cl<sub>8</sub>: A distorted kagome antiferromagnet, *J. Mater. Chem. C* **5**, 2629 (2017).
- [22] M. Hering, F. Ferrari, A. Razpopov, I. I. Mazin, R. Valentí, H. O. Jeschke, and J. Reuther, Phase diagram of a distorted kagome antiferromagnet and application to Y-kapellasite, *npj Comput. Mater.* **8**, 10 (2022).
- [23] T. Basu, F. Y. Wei, Q. Zhang, Y. Fang, and X. Ke, Complex magnetic structure in Ba<sub>5</sub>Ru<sub>3</sub>O<sub>12</sub> with isolated Ru<sub>3</sub>O<sub>12</sub>-trimer, *Phys. Rev. Mater.* **4**, 114401 (2020).
- [24] L. T. Nguyen and R. J. Cava, Hexagonal perovskites as quantum materials, *Chem. Rev.* **121**, 2935 (2021).
- [25] M. Azuma, T. Odaka, M. Takano, D. A. Vander Griend, K. R. Poeppelmeier, Y. Narumi, K. Kindo, Y. Mizuno, and S. Maekawa, Antiferromagnetic ordering of  $s = 1/2$  triangles in La<sub>4</sub>Cu<sub>3</sub>MoO<sub>12</sub>, *Phys. Rev. B* **62**, R3588 (2000).
- [26] Y. Qiu, C. Broholm, S. Ishiwata, M. Azuma, M. Takano, R. Bewley, and W. J. L. Buyers, Spin-trimer antiferromagnetism in La<sub>4</sub>Cu<sub>3</sub>MoO<sub>12</sub>, *Phys. Rev. B* **71**, 214439 (2005).
- [27] S. Wessel and S. Haas, Phase diagram and thermodynamic properties of the square lattice of antiferromagnetic spin-1/2 triangles in La<sub>4</sub>Cu<sub>3</sub>MoO<sub>12</sub>, *Phys. Rev. B* **63**, 140403 (2001).
- [28] L. Weber, N. Caci, and S. Wessel, Cluster quantum Monte Carlo study of two-dimensional weakly coupled frustrated trimer antiferromagnets, *Phys. Rev. B* **106**, 035141 (2022).
- [29] T.-T. Zhu, W. Sun, Y.-X. Huang, Z.-M. Sun, Y. Pan, L. Balents, and J.-X. Mi, Strong spin frustration from isolated triangular Cu(II) trimers in SrCu(OH)<sub>3</sub>Cl with a novel cuprate layer, *J. Mater. Chem. C* **2**, 8170 (2014).
- [30] P. Puphal, K. M. Zoch, J. Désor, M. Bolte, and C. Krellner, Kagome quantum spin systems in the atacamite family, *Phys. Rev. Mater.* **2**, 063402 (2018).
- [31] E. Dagotto and T. M. Rice, Surprises on the way from one- to two-dimensional quantum magnets: The ladder materials, *Science* **271**, 618 (1996).
- [32] C. Rojas-Dotti, N. Moliner, F. Lloret, and J. Martínez-Lillo, Ferromagnetic oxime-based manganese(iii) single-molecule magnets with dimethylformamide and pyridine as terminal ligands, *Crystals* **9**, 23 (2018).
- [33] J. Rodríguez-Carvajal, Recent advances in magnetic structure determination by neutron powder diffraction, *Phys. B: Condens. Matter* **192**, 55 (1993).
- [34] J. T. Haraldsen, T. Barnes, and J. L. Musfeldt, Neutron scattering and magnetic observables for  $s = 1/2$  spin clusters and molecular magnets, *Phys. Rev. B* **71**, 064403 (2005).
- [35] G. A. Bain and J. F. Berry, Diamagnetic corrections and Pascal's constants, *J. Chem. Educ.* **85**, 532 (2008).
- [36] J. Wang, M. Spitaler, Y.-S. Su, K. M. Zoch, C. Krellner, P. Puphal, S. E. Brown, and A. Pustogow, Controlled frustration release on the kagome lattice by uniaxial-strain tuning, *Phys. Rev. Lett.* **131**, 256501 (2023).
- [37] K. Caslin, R. K. Kremer, F. S. Razavi, A. Schulz, A. Muñoz, F. Pertlik, J. Liu, M.-H. Whangbo, and J. M. Law, Characterization of the spin- $\frac{1}{2}$  linear-chain ferromagnet CuAs<sub>2</sub>O<sub>4</sub>, *Phys. Rev. B* **89**, 014412 (2014).
- [38] V. A. Ivanshin, J. Deisenhofer, H.-A. Krug von Nidda, A. Loidl, A. A. Mukhin, A. M. Balbashov, and M. V. Eremin, ESR study in lightly doped La<sub>1-x</sub>Sr<sub>x</sub>MnO<sub>3</sub>, *Phys. Rev. B* **61**, 6213 (2000).
- [39] T. Gambke, B. Elschner, R. Kremer, and M. Schanz, Electron-spin-resonance of some rare-earths ions in cubic intermetallic compounds (AuCu<sub>3</sub>-structure), *J. Magn. Magn. Mater.* **36**, 115 (1983).
- [40] H. Benner, M. Brodehl, H. Seitz, and J. Wiese, Influence of nondiagonal dynamic susceptibility on the EPR signal of Heisenberg magnets, *J. Phys. C* **16**, 6011 (1983).
- [41] Z. Seidov, H.-A. Krug von Nidda, J. Hemberger, A. Loidl, G. Sultanov, E. Kerimova, and A. Panfilov, Magnetic susceptibility and ESR study of the covalent-chain antiferromagnets TlFeS<sub>2</sub> and TlFeSe<sub>2</sub>, *Phys. Rev. B* **65**, 014433 (2001).
- [42] S. El Shawish, O. Cépas, and S. Miyashita, Electron spin resonance in  $S = 1/2$  antiferromagnets at high temperature, *Phys. Rev. B* **81**, 224421 (2010).
- [43] H. Ikeuchi, H. De Raedt, S. Bertaina, and S. Miyashita, Size and temperature dependence of the line shape of ESR spectra of the XXZ antiferromagnetic chain, *Phys. Rev. B* **95**, 024402 (2017).
- [44] M. Heinrich, H.-A. Krug von Nidda, A. Krimmel, A. Loidl, R. M. Eremina, A. D. Ineev, B. I. Kochelaev, A. V. Prokofiev, and W. Assmus, Structural and magnetic properties of CuSb<sub>2</sub>O<sub>6</sub> probed by ESR, *Phys. Rev. B* **67**, 224418 (2003).
- [45] K. Kawasaki, Anomalous spin relaxation near the magnetic transition, *Prog. Theor. Phys.* **39**, 285 (1968).
- [46] D. L. Hubber, Critical-point anomalies in the electron-paramagnetic-resonance linewidth and in the zero-field relaxation time of antiferromagnets, *Phys. Rev. B* **6**, 3180 (1972).
- [47] M. S. Seehra, Role of anisotropy in the critical-point anomaly in EPR linewidth of MnF<sub>2</sub>, *Phys. Rev. B* **6**, 3186 (1972).
- [48] L. J. D. Jongh and A. R. Miedema, Experiments on simple magnetic model systems, *Adv. Phys.* **23**, 1 (1974).
- [49] E. Riedel and R. Willett, The temperature dependence of the angular variation of, and the critical point exponent for the EPR linewidth in the two-dimensional canted antiferromagnetic (C<sub>2</sub>H<sub>5</sub>NH<sub>3</sub>)<sub>2</sub>MnBr<sub>4</sub>: Evidence for a structural phase transition, *Solid State Commun.* **16**, 413 (1975).
- [50] P. M. Richards and M. B. Salamon, Exchange narrowing of electron spin resonance in a two-dimensional system, *Phys. Rev. B* **9**, 32 (1974).
- [51] S. Chehab, J. Amiel, P. Biensan, and S. Flandrois, Two-dimensional ESR behaviour of CrCl<sub>3</sub>, *Phys. B: Condens. Matter* **173**, 211 (1991).
- [52] D. V. Zakharov, J. Deisenhofer, H.-A. Krug von Nidda, P. Lunkenheimer, J. Hemberger, M. Hoinkis, M. Klemm, M. Sing, R. Claessen, M. V. Eremin, S. Horn, and A. Loidl, Spin dynamics in the low-dimensional magnet TiOCl, *Phys. Rev. B* **73**, 094452 (2006).